AD-A118 979 NAVAL RESEARCH LAB WASHINGTON DC F/G 20/5
THE NONLINEAR ASPECTS OF THE RAYLEIGH-TAYLOR INSTABILITY IN LAS--ETC(U)
SEP 82 M H EMERY, J H GARDNER, J P BORIS
UNCLASSIFIED NRL-MR-4882 NL

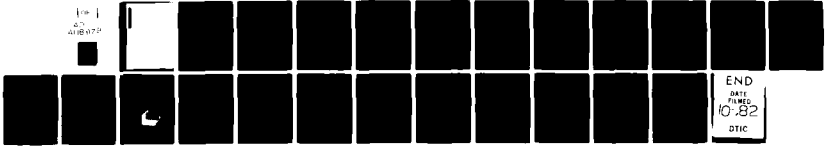

SECURITY CLASSIFICATION OF THIS PAGE (When Data Entered)

REPORT DOCUMENTATION PAGE	READ INSTRUCTIONS BEFORE COMPLETING FORM
1. REPORT NUMBER: NRL Memorandum Report 4882	2. GOVT ACCESSION NO.: AD-A118979
3. RECIPIENT'S CATALOG NUMBER	
4. TITLE (and Subtitle): THE NONLINEAR ASPECTS OF THE RAYLEIGH-TAYLOR INSTABILITY IN LASER ABLATION	5. TYPE OF REPORT & PERIOD COVERED: Interim report on a continuing NRL problem.
	6. PERFORMING ORG. REPORT NUMBER
7. AUTHOR(s): M.H. Emery, J.H. Gardner and J.P. Boris	8. CONTRACT OR GRANT NUMBER(s)
9. PERFORMING ORGANIZATION NAME AND ADDRESS: Naval Research Laboratory, Washington, DC 20375	10. PROGRAM ELEMENT, PROJECT, TASK AREA & WORK UNIT NUMBERS: DEAI088010; 44-1340-0-2
11. CONTROLLING OFFICE NAME AND ADDRESS: Department of Energy, Washington, DC 20545	12. REPORT DATE: September 3, 1982
	13. NUMBER OF PAGES: 23
14. MONITORING AGENCY NAME & ADDRESS(if different from Controlling Office)	15. SECURITY CLASS. (of this report): UNCLASSIFIED
	15a. DECLASSIFICATION/DOWNGRADING SCHEDULE

16. DISTRIBUTION STATEMENT (of this Report)

Approved for public release; distribution unlimited.

17. DISTRIBUTION STATEMENT (of the abstract entered in Block 20, if different from Report)

18. SUPPLEMENTARY NOTES

This research was supported by the U.S. Department of Energy.

19. KEY WORDS (Continue on reverse side if necessary and identify by block number)

Laser ablation
Rayleigh-Taylor
Kelvin-Helmholtz
Computational fluid dynamics
Hydrodynamic instabilities

20. ABSTRACT (Continue on reverse side if necessary and identify by block number)

We report on our investigation of the Rayleigh-Taylor (R-T) and Kelvin-Helmholtz (K-H) instabilities in laser ablatively accelerated targets for single mode perturbations for a series of wavelengths in the parameter regime $1/2 \leq \lambda/\Delta R \leq 10$, where λ is the wavelength of the perturbation and ΔR is the cold foil thickness. We find linear growth rates well below classical values (by a factor on the order of 3-4). We also find a cutoff in the

(Continues)

DD FORM 1 JAN 73 1473 EDITION OF 1 NOV 65 IS OBSOLETE
S/N 0102-014-6601

SECURITY CLASSIFICATION OF THIS PAGE (When Data Entered)

20. ABSTRACT *(Continued)*

growth rates for wavelengths less than the foil thickness. The striking result is the dominance of nonlinear effects; i.e., the K-H instability, for short wavelength perturbations. Although the linear growth rates increase as $k^{1/2}$ up to the cutoff, the K-H rollup dominates at large k, drastically reducing the penetration rate of the dense spike below its free fall value and effectively doubling the aspect ratio of the foil. In other words, it is the long wavelength perturbations that are most effective in destroying the symmetric implosion of the shell.

CONTENTS

THE NONLINEAR ASPECTS OF THE RAYLEIGH-TAYLOR INSTABILITY IN LASER ABLATION

INTRODUCTION

When a dense fluid is accelerated by a fluid of lower density the fluid interface is subject to the Rayleigh-Taylor (R-T)[1] instability. Any perturbation of the interface will grow in time and eventually form the nonlinear bubble-and-spike structure. In addition, the shear flow that develops as the bubble-and-spike structure evolves can lead to a Kelvin-Helmholtz (K-H)[2] like instability.

In general, it is not possible to separate these two basic interfacial instabilities because they interact; however, the R-T instability will dominate in the case of radically different densities (an Atwood number close to one) whereas K-H is more important when the densities are comparable (Atwood number close to zero). Both instabilities are expected to play a role in an unstably stratified fluid when the Atwood number (α) is in the range $0.25 \lesssim \alpha \lesssim 0.75$.

The R-T instability is a potential obstacle to inertial confinement fusion in that it causes corrugations in the ablation layer that eventually grow to form the nonlinear bubble-and-spike structure. The growth of small perturbations at the ablation layer will destroy the symmetry of high aspect ratio imploding shells.

We have previously reported on our investigation of the R-T and K-H instabilities in laser ablatively accelerated targets for a multi-wavelength perturbation of the ablation layer[3]. There we showed that the linear growth rates were well below classical values and a 20 μm thick plastic (CH) foil could be accelerated up to 160 km/s with a laser intensity of 10^{13} W/cm^2. We also showed that in the nonlinear regime strong velocity shear developed at

Manuscript submitted June 4, 1982.

the bubble-and-spike interface. This shear flow evolved into the nonlinear roll-up phase of the K-H instability which caused the tips of the spikes to widen and reduced their rate of "fall". The K-H instability thus served to stabilize the R-T instability.

There is a question of semantics involved in referring to the roll-up of the spike tips as the K-H instability. The roll-up of the spike tips is not due to a growing instability in the shear layer in the classical K-H sense and thus there is no linear growth rate associated with the roll-up. The roll-up of the spike tip is due to the accumulation of vorticity behind the head of the spike. This vorticity is generated by the baroclinic (non-collinear pressure and density gradients) nature of the flow and is advected down the sides of the spike. This accumulation of vorticity is similar to the nonlinear roll-up phase of the classical shear layer K-H instability. The roll-up of the R-T spike should more properly be referred to as a K-H-like mode.

Here we report on our investigation of the R-T and K-H-like instabilities for single mode perturbations for a series of wavelengths in the parameter regime $1/2 \leq \lambda/\Delta R \leq 10$, where λ is the wavelength of the perturbation and ΔR is the cold foil thickness. We again find linear growth rates well below classical values (by a factor on the order of 3-4). We also find a cutoff in the growth rates for wavelengths less than the foil thickness. The striking result is the dominance of nonlinear effects; i.e., the K-H roll-up, for the short wavelength perturbations. Although the linear growth rates increase as $k^{1/2}$ up to the cutoff, the K-H roll-up dominates at large k, drastically reducing the penetration rate of the dense spike below its free fall value and effectively doubling the aspect ratio of the foil. In other words, it is the long wavelength perturbations that are most effective in

destroying the symmetric implosion of the shell. The dominance of the nonlinear K-H roll-up and subsequent early saturation of the R-T instability for short wavelength perturbations was first postulated in Ref. 3.

II. MODEL

The R-T and K-H-like instabilities in laser ablatively accelerated targets are modeled using the FAST2D laser-shell simulation code [3,4,5]. This is a fully two-dimensional Cartesian code with a sliding Eulerian grid with variable grid spacing. The grid spacing is 0.25 μm for ten zones on either side of the ablation layer and increases uniformly to a 2 μm spacing for most of the rest of the grid. The finely zoned region near the ablation layer is required in order to accurately resolve the steep density gradient. The code has been run with a grid spacing as small as 0.10 μm with no noticeable difference in the results. The refined subzoning follows the ablation front throughout the course of the run. The zones in the underdense plasma beyond the critical surface and in the low-density rear portion of the foil are stretched. The system has 40 zones transverse to the laser beam (y direction) and 120 zones parallel (x direction). The system is periodic in the transverse direction.

FAST2D solves the ideal hydrodynamic equations using the flux-corrected transport (FCT)[6] algorithms with a two-dimensional classical ($T^{5/2}$) plasma thermal conduction routine. The initial density, pressure, and temperature profiles for a 20 μm-thick, plastic (CH) foil irradiated with an absorbed laser intensity I and laser wavelength of 1.05 μm are generated from a one-dimensional, analytic, quasistatic equilibrium model[7]. The analytic solutions have been shown to have provided an adequate steady state when FAST2D

is run in a one-dimensional mode[8], i.e., sans perturbation. There are only minor changes in the profiles [0(0.5%) change in the density gradient] after 1000 time steps (~ 3 ns). FAST2D also compares well with Naval Research Laboratory experimental data on hydrodynamic efficiencies, ablation pressures, and target velocities[8], with fluid blowoff profiles[9] and with beam nonuniformity effects [4]. A representative initial profile is illustrated in Fig. 1a and a two-dimensional perspective plot of the mass density is shown in Fig. 1b.

The initial perturbation is obtained by perturbing the density profile at its peak. A single sinusoidal mode is excited along the density peak corresponding to a total initial density perturbation of 2.3% $[(\rho_{max} - \rho_{min})/\langle\rho\rangle = 0.023]$.

III. NUMERICAL RESULTS

A typical result is illustrated in Fig. 2 where we plot the amplitude of the two most dominant modes for the 20 μm case ($\lambda/\Delta R=1$) with $I=1.0\times10^{13}W/cm^2$. M_K is the Fourier transform of the summed mass from the rear of the foil to the ablation edge for each transverse coordinate. The perturbed mode undergoes a very smooth exponential growth from 2.5 ns to 8 ns, saturates at about 10 ns and the foil fragments at about 14 ns. The rapid late time growth of the 30 μm mode is due to the coalescing of the vortices that form behind the heads of the spikes. There is no evidence of any substantial growth of the shorter wave-length modes. The growth of the shorter wavelength modes is suppressed because of the strong shear set up by the longer wavelength modes. This aspect of the problem is the subject of a future report.

The growth rates obtained when the systems are in the linear regime are compared with the classical value ($(kg)^{1/2}$) in Fig. 3. The growth rates are

approximately a factor of four below the classical value. The moderately strong cutoff appears for wavelengths less than the cold foil thickness.

The nonlinear development of the bubble-and-spike for $\lambda/\Delta R=1$ is illustrated in Fig. 4 where the density contours are plotted at four different times. The lines are contours of constant density in 10% increments of the maximum density counting from the outside inward. The laser is impinging the foil from the right. Strong rippling of the ablation layer is quite evident by 6.82 ns and the bubble-and-spike is well developed by 8.36 ns - at about the time the 20 μm mode is saturating. At 9.28 ns the lateral growth of the spike tip and the narrowing of the spike body is clearly apparent. Note that the rear of the target is quite uniform although the amplitude of the bubble-and-spike is on the order of 25 μm. As the spikes accelerate, lateral flow continues to widen the tips (10.26 ns).

The strong velocity shear and the vortex structures that develop behind the heads of the spikes are illustrated in Fig. 5 for the same four times. The solid lines are the 10% density contours. Note the strong circulatory flow (vortex flow) that builds up behind the heads of the spikes. These vortices are on the high density side of the 10% density contour and are typically entrained between the 10% and 30% contours and at times between the 20% and 40% contours. This gives an Atwood number of 1/2 to 1/3-well within the range for the appearance of the K-H instability.

The strong spiral roll-up obtained by other researchers[10,11,12] simulating the R-T and K-H instabilities in incompressible, two fluid systems with a well defined interface and constant acceleration is not in evidence here. This is due to the finite density gradients, ablation and compressibility effects; however, the widening and rounding of the spike tips, the flattening of the rear of the spike (due to the reversed flow there) and the

vortices at the rear of the spike are all definitive signatures of the K-H instability.

The ablation region becomes quite turbulent before the foil fractures as shown in Fig. 6. The density contours at 11.27 ns are illustrated in Fig. 6a. The spikes are beginning to break apart and the bubbles have been sealed off. The corresponding fluid flow is shown in Fig. 6b. The vortices have coalesced to form two very large vortex structures and hence the rapid late time growth of the 30 μm wavelength mode.

The nonlinear evolution of the R-T instability is qualitatively similar for perturbed wavelengths in the range $1/2 < \lambda/\Delta R < 1.25$: the linear growth of the perturbed mode begins to deviate from its exponential character when the amplitude of the bubble-and-spike (as measured from the top of the bubble to the head of the spike using the 30% density contour) is equal to approximately half the wavelength of the peturbation. At this time the vortices begin collecting behind the head of the spikes, widening the spike tips and slowing the growth of the R-T instability while the rear of the foil remains laminar and is accelerated uniformly.

Since the linear growth of the perturbed mode does not begin to saturate, nor do the vortex signatures appear, until the perturbation reaches an amplitude of half the wavelength, one might expect the nonlinear evolution of the long wavelength perturbations to be quite different from the short wavelength perturbations. Indeed such is the case. The density contours and fluid flow vectors for the 50 μm perturbation at 9.45 ns are illustrated in Figs. 7a and 7b. There is, as yet, no evidence of spike-tip widening and, in fact, most of the foil mass is in the spikes and the rear of the foil is severely distorted (the left most contour is the 30% density contour). There is only a hint of a very weak vortex buildup along the side of the spike.

Thus although the linear growth rates of the long wavelength perturbations are less than that for the short wavelength perturbations, the nonlinear evolution is strikingly different and the foil actually fractures much earlier in time with the long wavelength perturbations.

The linear and nonlinear aspects of the R-T instability can be differentiated by examining the amplitude of the bubble-and-spike as a function of time. Fig. 8 shows the logarithm and square root of the bubble-and-spike amplitude as a function of time for the 20 μm wavelength mode. The linear (exponential) growth begins to saturate at about 8 ns and the spike goes into "free-fall" with the amplitude very well described by $A = 1/2"g"t^2$ where "g" is the "free-fall" acceleration. The spike goes into "free-fall" when the amplitude (A) of the disturbance is on the order of 1/5 the wavelength [$A \sim 0(0.2\lambda)$]. This early departure from linear theory is in agreement with simulations of the classical two-fluid R-T instabiilty[11,12], but departs from the commonly held belief that nonlinear effects are not important until $A \sim 0(0.4\lambda)$.

This shift from exponential growth to quadratic growth is qualitatively similar for all the wavelengths investigated. Quantitatively, however, the results are critically dependent on the wavelength. The amplitude of the large wavelength modes ($\lambda/\Delta R > 1.25$) goes into "free-fall" at a later time and with an effective "free-fall" acceleration comparable to the foil acceleration [$0(1.5\times10^{15}$ cm/s^2)]. The exponential growth of the short wavelength modes ($\lambda/\Delta R \lesssim 1.25$) saturates more than 2 ns earlier in time and the "free-fall" acceleration of the spike is reduced by more than a factor of two over the long wavelength modes. This reduced rate of penetration of the dense spike below its "free-fall" value is a direct consequence of the tip-widening brought on by the K-H instability. The frontal area of the

spike is increased thereby increasing its drag and reducing its rate of fall.

These results have serious implications with respect to shell integrity as a function of perturbation wavelength. This is evident from Fig. 9 where both the "free-fall" acceleration of the spike and the final aspect ratio of the foil are plotted as a function of perturbation wavelength ($\lambda/\Delta R$). Note that the "free-fall" acceleration ("g") of the spike is reduced by over a factor of two for the short wavelengths. As a result of the reduced "free-fall" and the earlier saturation of the exponential growth the aspect ratio ($R/\Delta R$) of the short wavelength perturbation has been increased by a factor of two over the long wavelength modes. ΔR is the cold foil thickness (20 μm) and R is the distance traveled by the foil up to the time at which at least 65% of the foil mass remained and/or the rear of the foil was still being accelerated uniformly. The solid circles are the aspect ratios obtained with a laser intensity of 5.0×10^{13} W/cm^2, where the same effect is evident. The # symbol is the aspect ratio obtained for a 200 μm perturbation ($I = 1.0\times10^{13}$ W/cm^2) and as one would intuitively guess the aspect ratio increases again for wavelengths very much larger than the foil thickness. Thus although the linear growth rate increases as $k^{1/2}$, up to the cutoff, non-linear effects, in the form of the K-H roll-up, are quite effective in saturating the R-T instability, reducing the rate of "fall" of the spike and increasing the lifetime of the foil. The physical mechanism for the cutoff is the subject of a future report now in preparation.

III. SUMMARY AND CONCLUSIONS

We have extended our previous investigation of the multimode structure of the R-T and K-H instabilities in ablatively accelerated targets to that of

the linear and nonlinear nature of the single mode structure. The linear growth rates are well below the classical $(kg)^{1/2}$ value and a cutoff appears for wavelengths less than the cold foil thickness.

The K-H instability plays a very dominant role for $\lambda/\Delta R \lesssim 1.25$. The strong vortex structure that builds up behind the heads of the spikes causes the tips of the spikes to widen thus reducing their rate of fall. The increased drag effectively doubles the aspect ratio for the short wavelength perturbations. In short, it is the longer wavelength modes ($2 \lesssim \lambda/\Delta R \lesssim 8$) that are the most dangerous since they are the most effective at destroying the spherical symmetry of the imploding shell.

The fact that the long wavelength perturbations are the most dangerous modes with respect to hydrodynamic instabilities raises again the specter of laser asymmetries. We have previously shown that laser asymmetries with scalelengths greater than the distance from the ablation surface to the critical surface would have a severe impact on drive pressure symmetry and hence on pellet gain[4]. It is now apparent that these long wavelength asymmetries are relatively more dangerous than previously thought since, hydrodynamically, they lead to an earlier fracture of the target than shorter wavelengths do. In this context, however, it is important to remember that the growth rates are well below classical values.

ACKNOWLEDGEMENTS

The authors thank S. Bodner, J. Grun and R. Whitlock for the valuable conversations and the support of the Laser Plasma Branch at NRL is gratefully appreciated. One of us (MHE) gratefully acknowledges the many stimulating discussions with A.L. Cooper and M.J. Fritts. This research was supported by the U.S. Department of Energy.

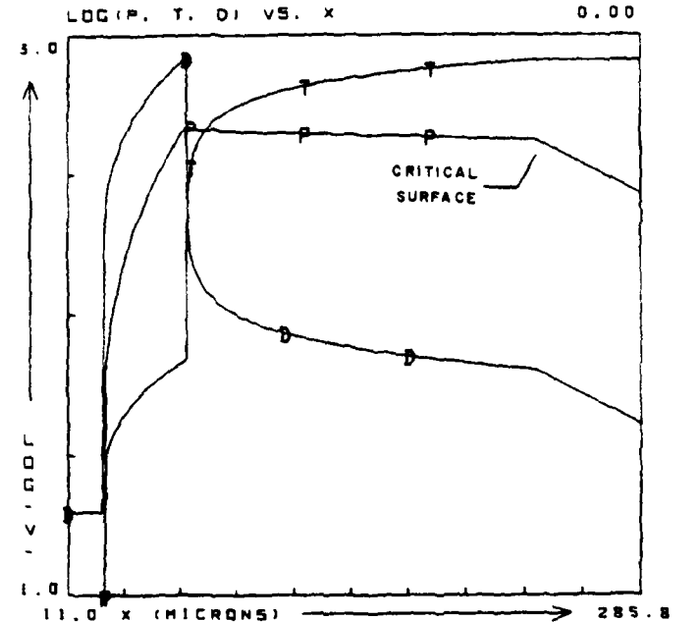

(a)

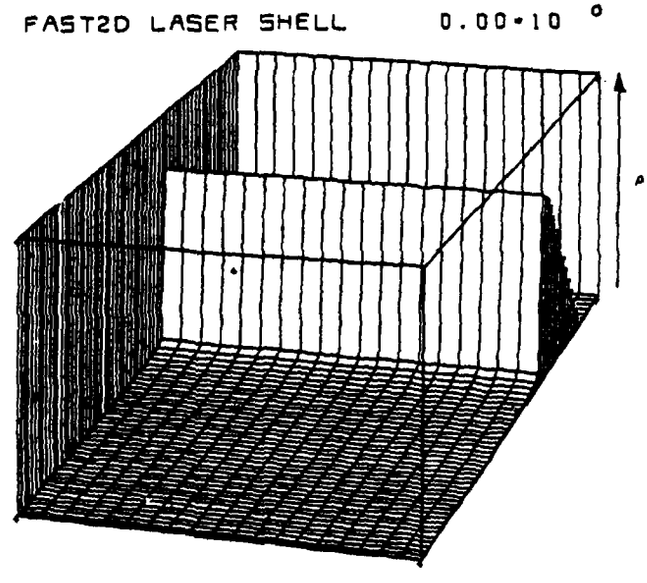

(b)

Fig. 1 — (a) A semi-log plot of the initial pressure, density and temperature profiles of a thin plastic foil. (b) A two-dimensional perspective plot of the initial mass density. The laser is coming in from the front.

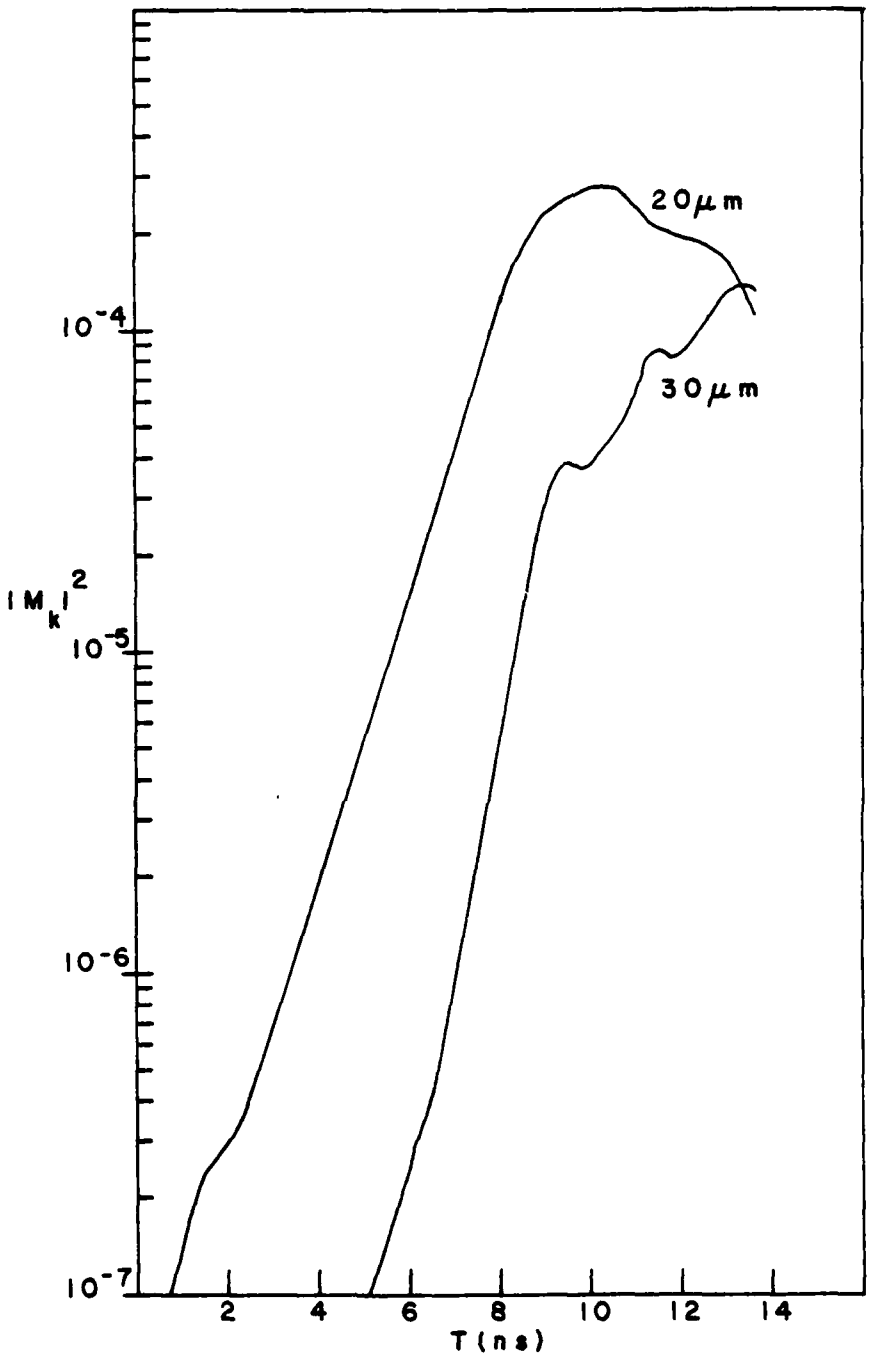

Fig. 2 — The square of the amplitude of the two most dominant modes as a function of time. The 20 μm mode is the perturbed mode.

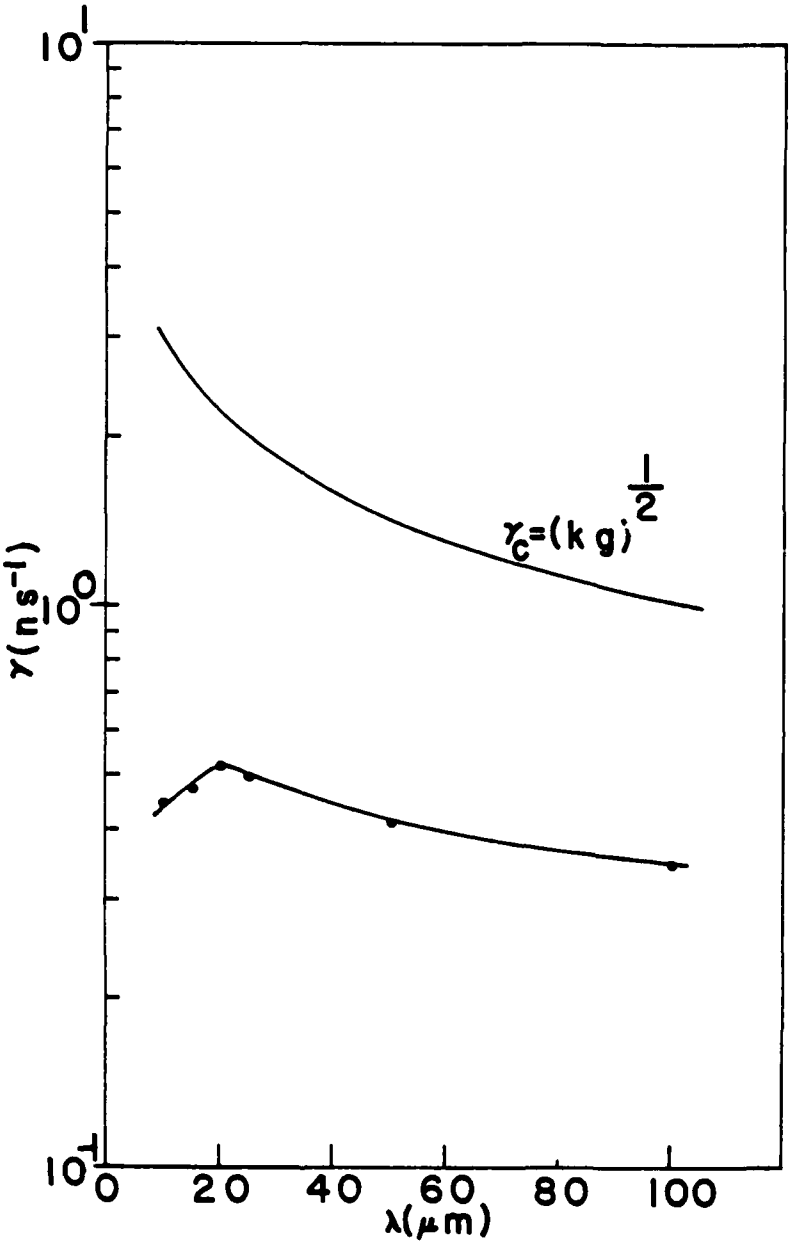

Fig. 3 — A comparison of the growth rates when the systems are in the linear regime to the classical value ($(kg)^{1/2}$).

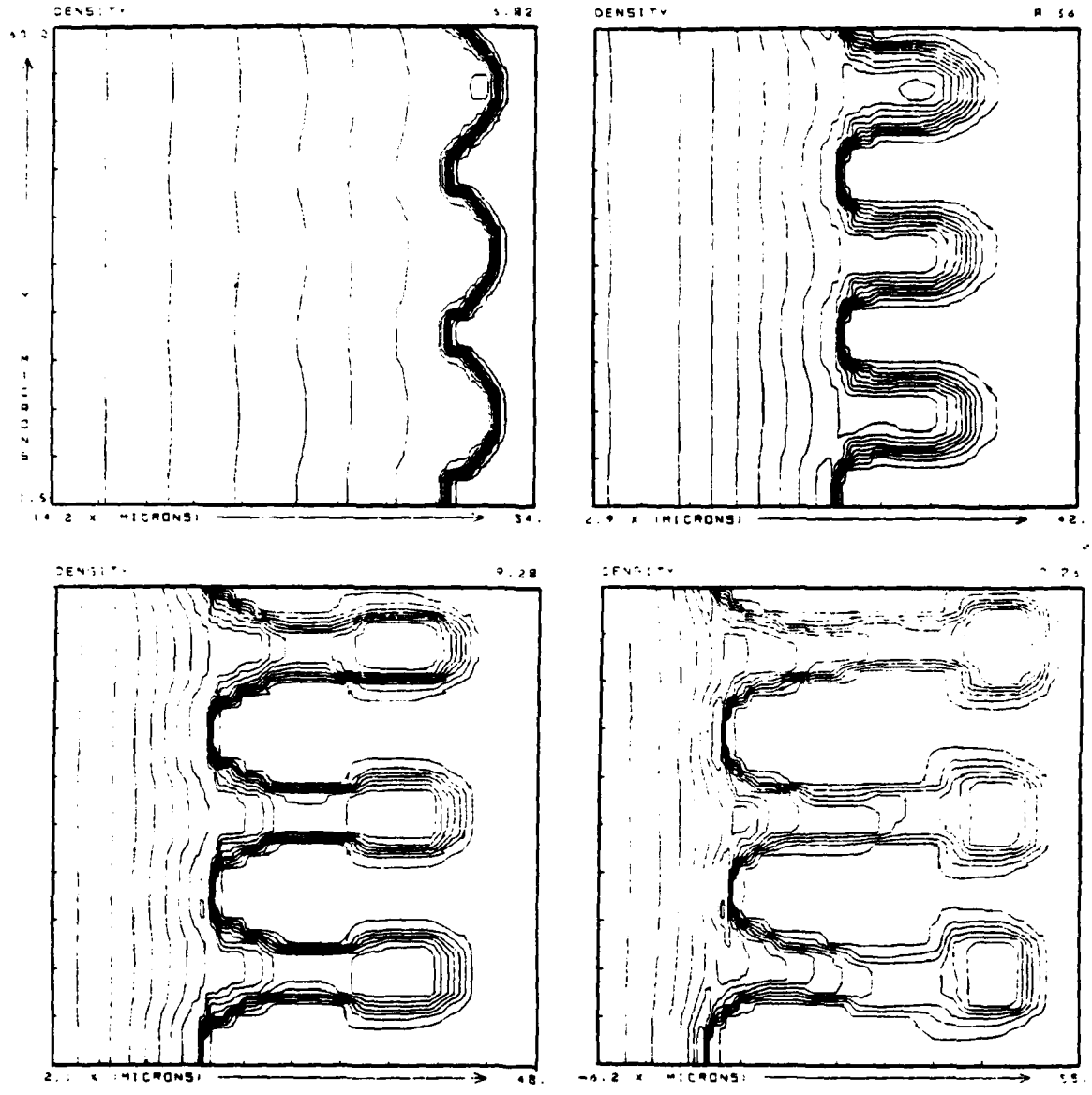

Fig. 4 — Density contours at different times showing the nonlinear development of the bubble-and-spike and the subsequent tip-spreading. The contours are in 10% increments of the maximum density ($\rho_{max} \approx 0.80$ gm/cm^3) counting from the outside inward. The laser is coming in from the right.

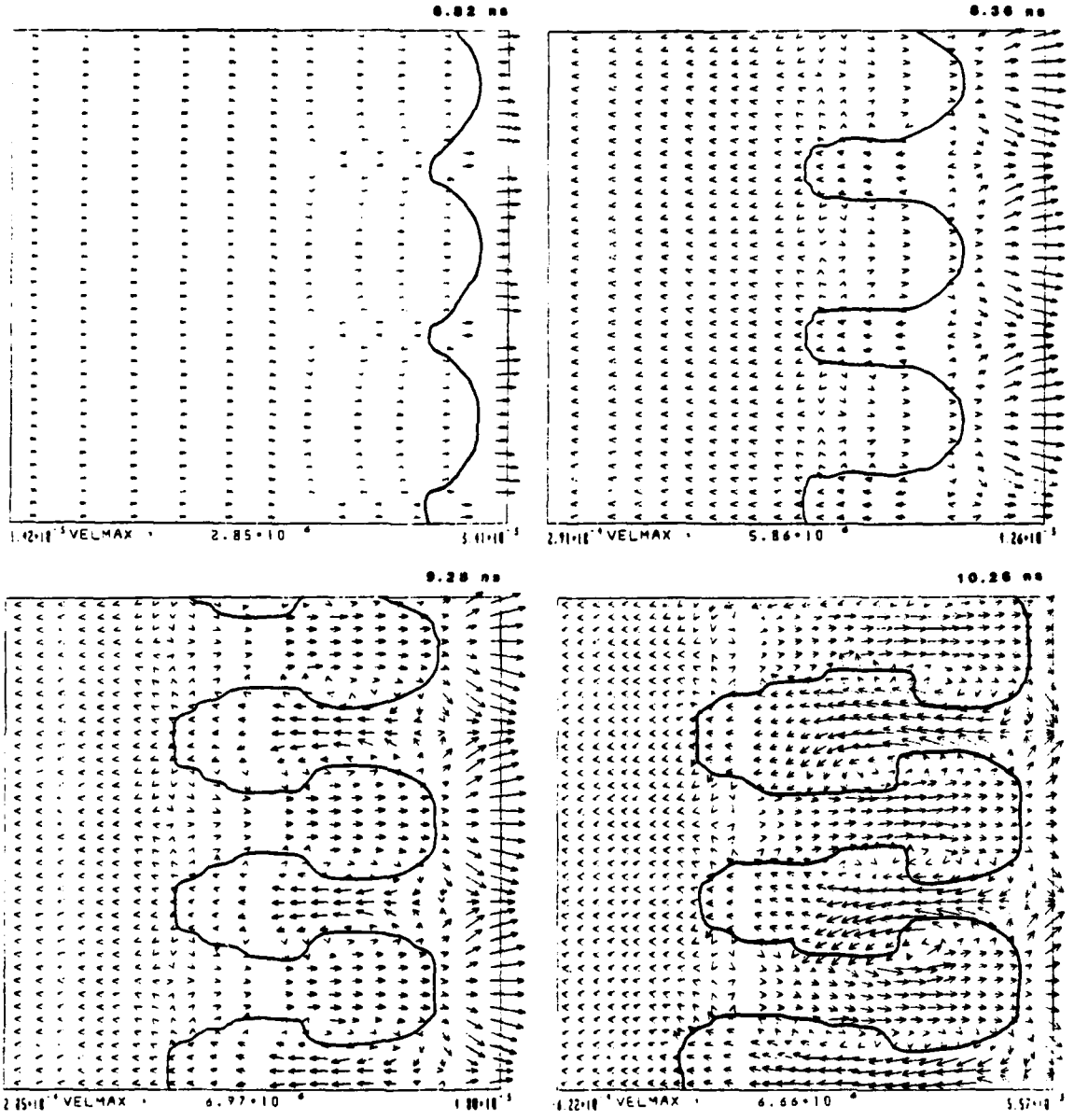

Fig. 5 — Fluid velocity vector plots for the same times and regions in space as Fig. 4. The solid line is the 10% density contour. Velmax is the maximum velocity in the range plotted. The vortex structures behind the heads of the spike are quite evident.

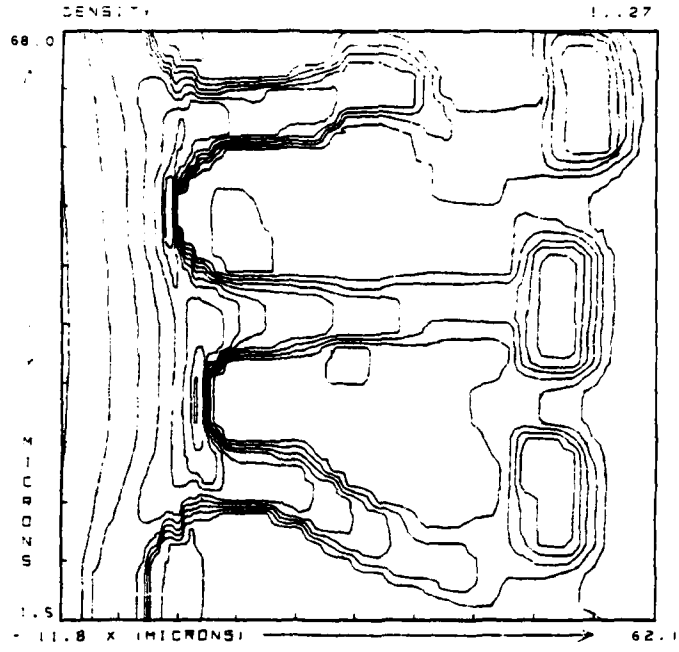

(a)

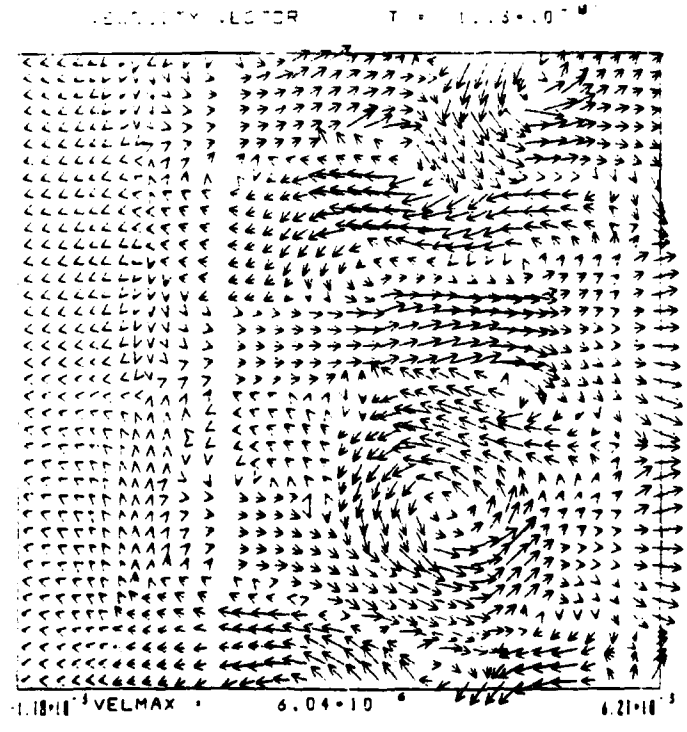

(b)

Fig. 6 — (a) Density contours for the 20 μm perturbation at 11.27 ns. The spikes are beginning to fracture and the bubble has been sealed off. (b) Fluid velocity vector plots at the same time illustrating the coalescing of the small vortices into two very large vortices.

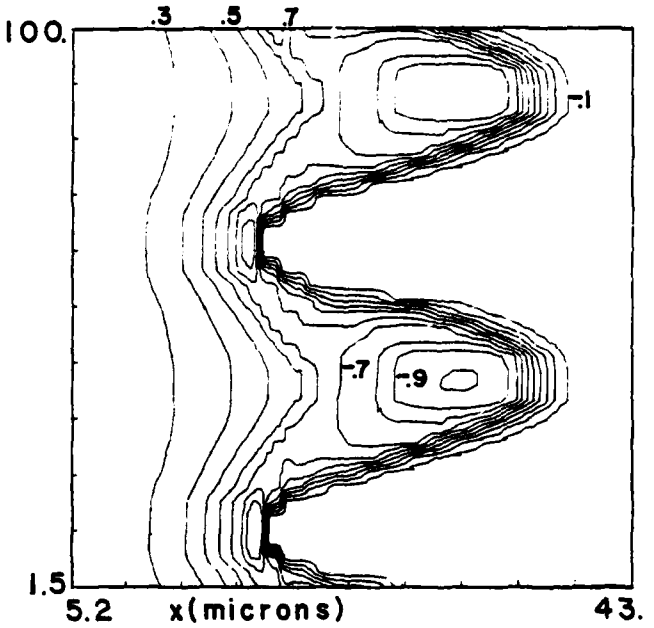

(a)

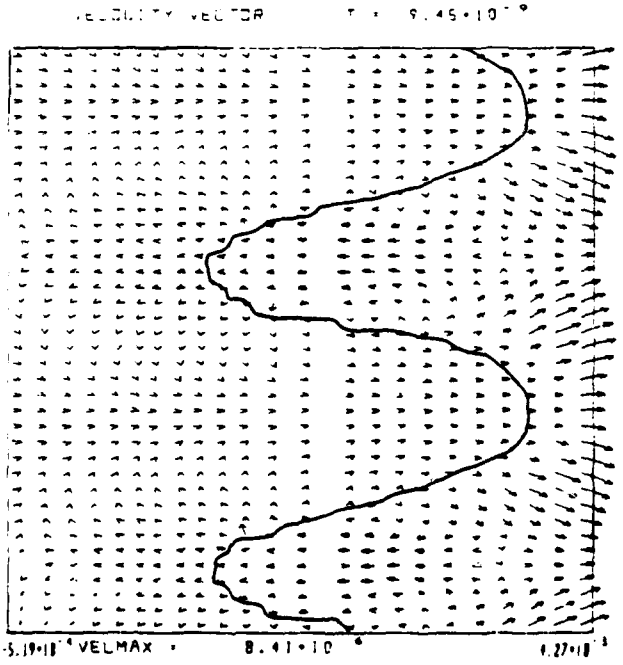

(b)

Fig. 7 — (a) Density contours at 9.45 ns for the 50 μm perturbation. Most of the foil mass is in the spike tips and there is no evidence of any tip-widening. (b) Velocity vector plots of the same time illustrating the lack of strong vortex formation.

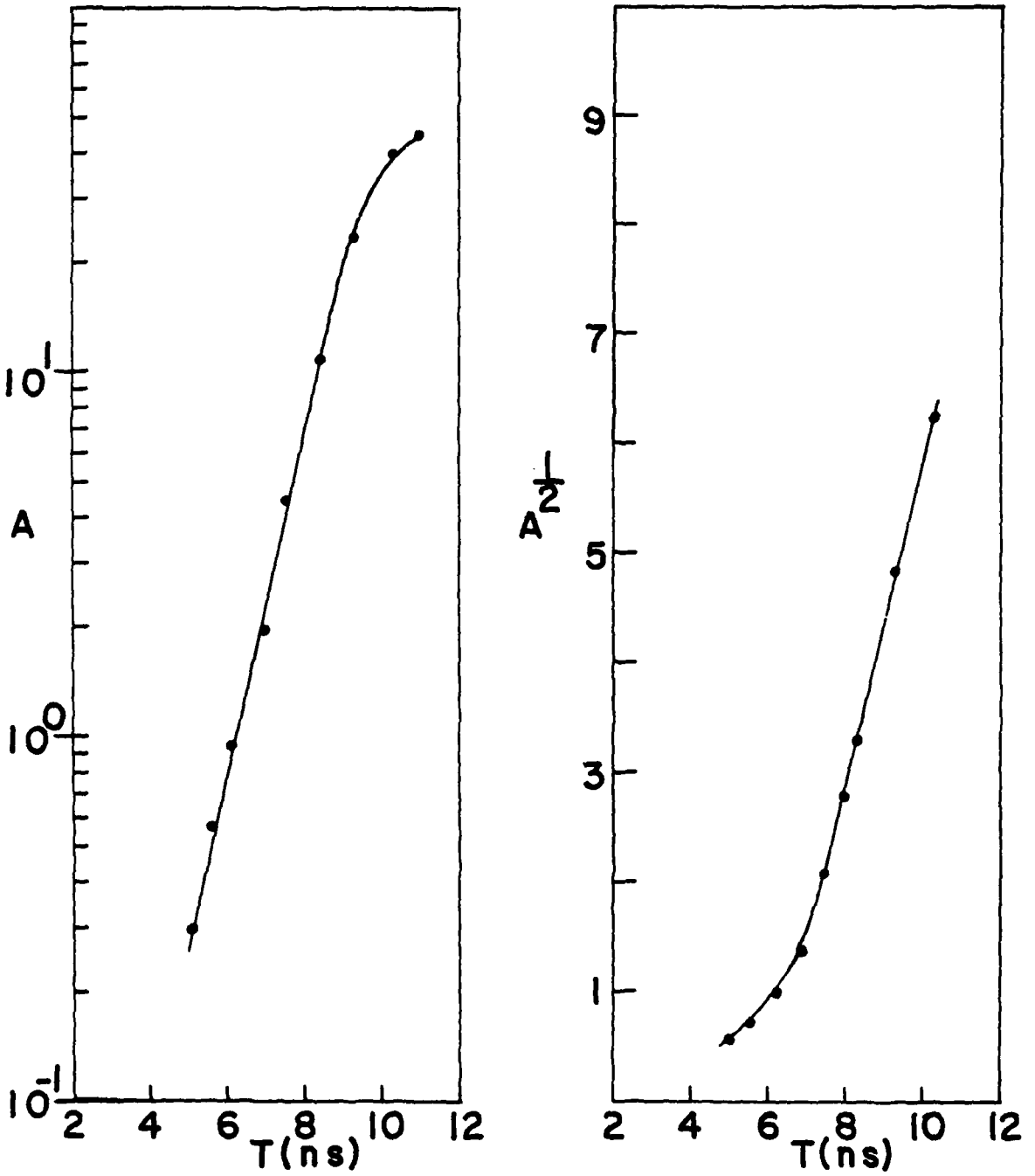

Fig. 8 — A plot of the lnA and $A^{1/2}$, where A (in μm) is the amplitude of the bubble and spike, for the 20 μm mode. The slope of $A^{1/2}$ yields the "free-fall" acceleration of the spike.

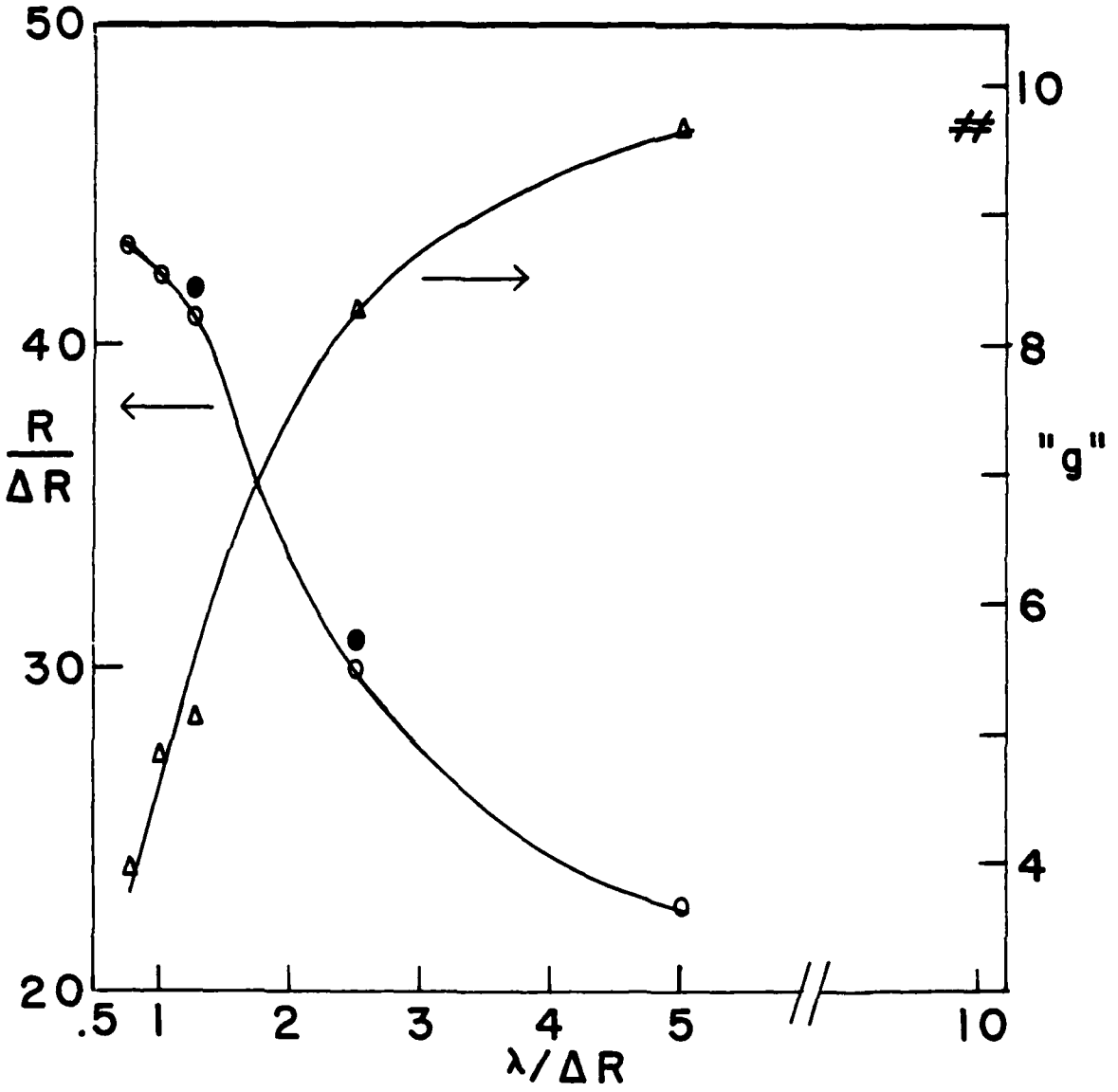

Fig. 9 — A plot of the "free-fall" acceleration ("g" in units of 10^{14} cm/s^2) of the spike and the final aspect ratio of the foil as a function of the perturbation wavelength ($\lambda/\Delta R$). The solid circles are the aspect ratios obtained with a laser intensity of 5×10^{13} W/cm^2 and the # symbol is the aspect ratio obtained with a perturbation wavelength of 200 μm.

REFERENCES

1. Lord Rayleigh, Theory of Sound 2nd ed., 1894 (Dover Publications, Inc., New York, 1945), Vol. 2, G. Taylor, Proc. Roy. Soc. (London) 201, Series A, 192 (1950).
2. H. Helmholtz, Phil. Mag., Ser. 4, 36, 337 (1868); Lord Kelvin, Hydrodynamics and General Dynamics (Cabridge University Press, Cambridge, 1910), p. 69ff.
3. M.H. Emery, J.H. Gardner and J.P. Boris, Phys. Rev. Lett. 48, 677 (1982).
4. M.H. Emery, J.H. Orens, J.H. Gardner and J.P. Boris, Phys. Rev. Lett. 48, 253 (1982).
5. J.P. Boris, Comments on Plasma Physics and Controlled Fusion 3.1 (1977).
6. J.P. Boris and D.L. Book, Methods of Comp. Phys. 16, 85 (1976).
7. J.H. Orens, NRL Memo Report 4167 (1980).
8. P.H. Moffa et al., Bull. Am. Phys. Soc. 24, 946 (1979); NRL Laser-Plasma Interaction Group, NRL Report No. 4369, 1980.
9. M. Herbst et al., Bull. Am. Phys. Soc. 26, 1024 (1981).
10. M.J. Fritts et al., Computer Methods in Fluids (Pentech Press, London, 1980).
11. G.R. Baker et al., Phys. Fluids 23, 1485 (1980).
12. B.J. Daly, Phys. Fluids. 10, 297 (1967).